Available online at www.sciencedirect.com
SCIENCE DIRECT®
Journal of Electroanalytical Chemistry 554–555 (2003) 449–458
Journal of Electroanalytical Chemistry
www.elsevier.com/locate/jelechem

Manipulation of the distance of light-induced electron transfer within a semi-rigid donor(amine)/acceptor(terpyridine) assembly via complexation of di-positive and tri-positive metal ions

Keith A. Walters, Young-Jin Kim, Joseph T. Hupp *

Department of Chemistry, Northwestern University, Evanston, IL 60208-3113, USA

Received 14 December 2002; received in revised form 28 March 2003; accepted 25 April 2003

Dedicated to the memory of Prof. Michael J. Weaver

Abstract

Electric field-effect spectroscopy techniques (electronic absorption and emission) have been applied to the problem of light-induced electron transfer (ET) within a covalently linked organic donor/acceptor pair. The spectroscopy measurements report on the change in the assembly's dipole moment upon ET. This quantity (the dipole-moment change) represents a direct measure of the distance over which the electron is transferred. The experiments show that the true charge transfer distance is much less than the geometric separation distance between the nominal electron donor and acceptor centers. The experiments additionally show that the transfer distance can be changed: binding of both open-shell and closed-shell metal cations with the acceptor portion of the assembly causes the ET distance to increase, with a tri-positive ion inducing a greater increase than di-positive ions. Electronic structure calculations qualitatively reproduce the experimental observations. From the calculations, the lengthening of the transfer distance is an electrostatic effect that appears to be associated primarily with a change in the shape of the orbital occupied by the transferred electron in the redox product state.

Keywords: Light-induced electron transfer; Electric field-effect spectroscopy; Charge transfer distance

1. Introduction

Mike Weaver had a longstanding interest in the kinetics and dynamics of electron transfer (ET) reactions, including reactions in homogeneous solution environments. Beginning with his postdoctoral studies at Caltech with Prof. Fred Anson and continuing as a major component of his early independent scientific career at Michigan State University and Purdue University, Mike made numerous enlightening contributions. The problems that interested him ranged from classic kinetic double-layer effects [1] to electron tunneling phenomena [2] and solvent dynamical effects [3]. Here we describe a case study of a question that is implicit in nearly all ET kinetics and dynamics studies: 'how far is the electron transferred?' At first glance, this would appear to be a trivial question, given a knowledge of the location and arrangement of the atoms comprising the reacting redox species (for example, from high-level molecular modeling, or better still, from direct structural measurements). Several experimental and computational studies have shown, however, that true ET distances can differ substantially from the simple geometric distance defined by the donor-center/acceptor-center separation distance—true distances typically being significantly shorter [4–12]. The origins of the discrepancies have been traced to self-polarization, partial charge delocalization, and mixing of reactant or product electronic states with upper electronic states

* Corresponding author. Tel.: +1-847-491-3504; fax: +1-847-491-7713.
E-mail address: jthupp@chem.nwu.edu (J.T. Hupp).

0022-0728/03/$ - see front matter © 2003 Elsevier Science B.V. All rights reserved.
doi:10.1016/S0022-0728(03)00315-2

(non-charge transfer states), among other effects [13–15]. Additionally, it has been recognized that discrepancies can reflect the limitations inherent in applying one-electron theories (Hush, Mullikan, Marcus) to real chemical or electrochemical systems featuring multiple valence electrons (albeit, only one transferring electron).

The reaction we chose to examine was a light-induced intramolecular charge transfer. As indicated in Eq. (1), a pendant tertiary amine serves as an electron donor and one or more pyridyl nitrogen atoms serve as electron acceptors. Inclusion of ethylene spacers makes half the molecule's aromatic rings coplanar and creates extended conjugated pathways between the electron donor and acceptors. The conjugation and resulting good electronic communication are manifest as an intense visible-region charge transfer absorption band. The system can be made more fully coplanar and the strength of the pyridyl nitrogen atoms as electron acceptors can be significantly enhanced by chelating a metal cation with the available set of three pyridines. The enhanced electron accepting ability of the coordinated nitrogen atoms is manifest experimentally as a shift in the charge transfer absorption maximum to lower energy. As emphasized in particular by Zyss and co-workers, one potential application of coordination complexes of molecules similar to that in Eq. (1) is as

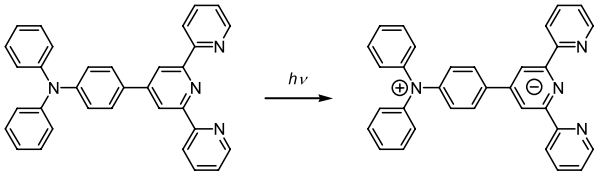

(1)

nonlinear optical chromophores [16]. Hyper-Rayleigh scattering measurements, e.g. show that several of the complexes feature very large first hyperpolarizabilities, i.e. coefficients for optical frequency doubling [16]. The large hyperpolarizabilities are a direct consequence of visible-region accessibility of intense charge transfer absorption bands.

Light absorption was of interest to us for a different reason: it makes possible the application of electric field-effect (Stark effect) spectroscopy techniques [17]. When applied to charge transfer transitions, these techniques are capable of reporting on the true ET distance (i.e. light-induced charge transfer distance). An alternative technique, transient dc photoconductivity, is useful for neutral compounds, but cannot be applied to charged compounds [8]. Other limitations of the alternative approach include collinearity of the transition dipole-moment and change-in-dipole-moment vector, and significant (>0.3 ns) charge transfer state lifetimes. As explained further below, it is sometimes advantageous to apply Stark methods not only to absorption processes, but also to light emission, i.e. the reverse of Eq. (1):

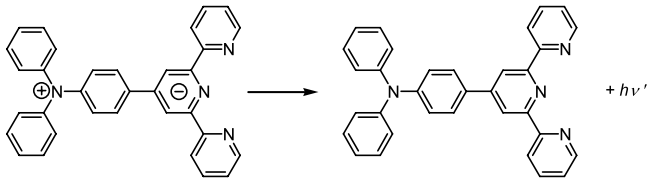

(2)

We have used electro-absorption and electro-emission techniques to determine true intramolecular ET distances (adiabatic distances, R_{12}) for light-induced reactions within the compound in Eqs. (1) and (2). We have examined the free compound as well as four coordination complexes. We find that the true transfer distance is, in all cases, considerably smaller than the geometric donor/acceptor separation distance, R_{geo}. We additionally find that the true transfer distance, but not the geometric separation distance, changes significantly upon metal ion coordination. We also find that the adiabatic intramolecular ET distance can be altered based on the charge of the nominally innocent, peripherally coordinated metal cation. Finally, we find that the experimentally observed distance-alteration effects are replicated qualitatively by semi-empirical electronic structure calculations.

2. Background

Stark spectroscopy involves the evaluation of electric field effects upon chromophore properties—in our case a molecule's electronic absorption or emission spectrum. As implemented here, electroabsorption experiments involve isotropic solutions of chromophores. By employing a rigid matrix such as a polymer film or a low-temperature organic glass, the random orientation of chromophores can be preserved in the presence of an electric field. The expected effect of an applied field upon this kind of sample is shown schematically in Fig. 1. Assuming that the chromophores have nonzero

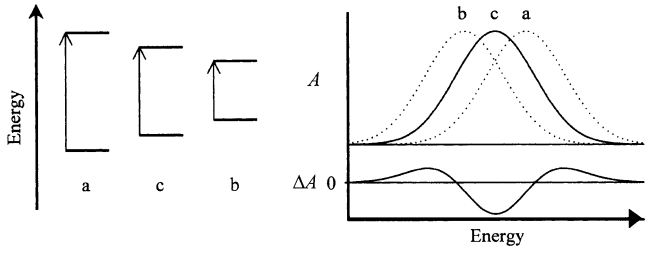

Fig. 1. Schematic representation of electroabsorption experiment for a frozen isotropic sample. Cases a, b and c correspond to parallel, antiparallel, and perpendicular orientations of the ground state molecular dipole with respect to the applied electric field. The excited state dipole is assumed to be oriented opposite to the ground state dipole. Under these conditions, an applied electric field will symmetrically broaden the absorption spectrum such that the difference spectrum (field on–field off) has a second-derivative shape.

ground state dipole moments, the applied field will: (a) stabilize those with dipoles aligned parallel to the field, (b) destabilize those with dipoles aligned antiparallel to the field, and (c) exert no effect upon those aligned perpendicular to the field. If optical excitation results in a change in molecular dipole moment—say, a reversal in sign due to substantial donor-to-acceptor charge transfer—the field will: (a) destabilize photo excited molecules whose dipole moments are now oriented antiparallel to the field, (b) stabilize the excited states of those molecules now oriented parallel to the field, but (c) exert no effect upon those aligned perpendicular to the field. Case a (stabilization of the ground state and destabilization of the excited state) will be manifest as a shift in absorbance band to higher energy. Case b will be manifest as a shift in absorbance to lower energy. Case c will yield no spectral shift. The overall effect expected is a broadening of the spectrum at the expense of extinction at its center; Fig. 1. Taking the difference in absorption spectra with and without the field (the 'Stark spectrum'), a second-derivative lineshape with respect to the original spectrum should result.

Another effect of the field will be to stabilize the chromophores simply by polarizing their electron clouds; in other words an induced dipole effect will exist. Clearly, the greater the degree of electronic polarizability the greater is the degree of stabilization. If the polarizability of the chromophore in an excited state differs from its polarizability in the ground state, then the amount of stabilization induced will likewise differ. For example, if the excited state is more polarizable than the ground state, the upper state will be preferentially stabilized energetically and a spectral red shift would be expected. If the excited state is less polarizable, then a blue shift is expected. Note that the effects are independent of the orientation of the molecule with respect to the field. Consequently, the individual absorption spectra of all the chromophores comprising the sample will be shifted in the same direction (either to lower or higher energy). Taking the difference in absorption spectra with and without the field, a first-derivative contribution to the lineshape, relative to the field-free spectrum, is expected; Fig. 2.

In general, a combination of first- and second-derivative contributions to the Stark spectrum can be expected. If, in addition, the application of a field changes the 'allowedness' of a transition (e.g. by mixing upper excited states or otherwise relaxing an unfavorable selection rule), the overall absorption band intensity will change and a zeroth-derivative contribution can be expected. Notably, the magnitude of the Stark signal, regardless of its origin, scales as the square of the applied electric field (Eq. (3), below). High fields are achieved experimentally by using short pathlengths and a sinusoidally alternating high-voltage source. The alternating source diminishes the opportunity for dielectric breakdown of the sample while, at the same time, making the experimental output readily amenable to lock-in amplification.

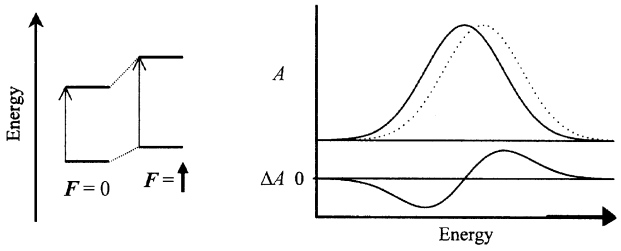

Fig. 2. Schematic representation of polarizability effects in an electroabsorption absorption experiment. If the randomly oriented molecules comprising the sample experience an increase in polarizability upon charge transfer excitation, a red shift will occur in the presence of an applied electric field. The difference spectrum will have a first-derivative shape.

As described more quantitatively below, *the key feature of the Stark experiment is the extraction of the ground state/excited state dipole moment change because this quantity can be related directly to the absolute distance of light-induced intramolecular ET* [18].

3. Analysis

Analysis of electroabsorption spectra was performed using Liptay's approach [17], exhaustively described elsewhere [9] and only briefly summarized here. Consistent with the description above, each electroabsorption spectrum (r.m.s. difference spectrum: field on–field off; $\Delta A(v)$) was fit to a linear combination of the frequency-weighted (v-weighted) zeroth, first, and second derivatives of the unperturbed absorption spectrum, $A(v)$:

$$\Delta A(v) = \left\{ A_\chi A(v) + \frac{B_\chi v}{15hc}\frac{\mathrm{d}[A(v)/v]}{\mathrm{d}v} + \frac{C_\chi v}{30h^2c^2}\frac{\mathrm{d}^2[A(v)/v]}{\mathrm{d}v^2} \right\} \boldsymbol{F}_{\mathrm{int}}^2 \tag{3}$$

In Eq. (3), h is Planck's constant, c is the speed of light in vacuum, and $\boldsymbol{F}_{\mathrm{int}}$ is the internal electric field experienced by the chromophore. $\boldsymbol{F}_{\mathrm{int}} = f\boldsymbol{F}_{\mathrm{external}}$, where f is a local field correction factor. For a spherical cavity, if the molecularity of the solvent is ignored, f can be approximated as $3D_s/(2D_s+1)$ where D_s is the static dielectric constant of the glass or solvent. On this basis Karki and Hupp [9] have estimated f(butyronitrile) to be ~ 1.3. Ponder and Matthies have estimated f(PMMA) to be 1.11 [19].

From the discussion above, the coefficient A_χ provides information about electric field-induced changes in the transition dipole moment; B_χ, and C_χ provide information about absorption-induced changes in mo-

lecular polarizability and dipole moment, respectively. The coefficients are given by:

$$A_\chi = \frac{\langle \alpha_m \rangle}{3} + \frac{1}{30}(3\cos^2\chi - 1)[3\langle \beta_m \rangle - 2\langle \alpha_m \rangle] \quad (4)$$

$$B_\chi = \frac{5}{2}\mathrm{Tr}\Delta\alpha + (3\cos^2\chi - 1)\left(\frac{3}{2}\hat{\boldsymbol{g}}\cdot\Delta\alpha\cdot\hat{\boldsymbol{g}} - \frac{1}{2}\mathrm{Tr}\Delta\alpha\right) \quad (5)$$

$$C_\chi = |\Delta\mu|^2[5 + (3\cos^2\zeta - 1)(3\cos^2\chi - 1)] \quad (6)$$

In the equations, α_m and β_m are the scalar portions of the polarizability and hyperpolarizability tensors, χ is the angle between the incident electromagnetic field and the applied electrical field vectors, $\mathrm{Tr}\Delta\alpha$ is the trace of the polarizability difference between excited and ground electronic states, $\hat{\boldsymbol{g}}\cdot\Delta\alpha\cdot\hat{\boldsymbol{g}}$ is the polarizability change along the transition dipole moment vector ($\hat{\boldsymbol{g}}$ is the unit vector), and ξ is the angle between the transition dipole moment and change-in-dipole-moment vectors.

The analysis used for electro-emission data is described elsewhere [8]. Briefly, however, it closely parallels the electro-absorption analysis. The electro-emission experiment is especially attractive in those cases where bands in the corresponding absorption spectrum overlap significantly. If bands overlap, the reliability of the electro-absorption analysis depends critically upon the quality of the deconvolution of the overlap. Because emission tends to occur exclusively from the lowest electronic excited state, only a single emission band is observed and deconvolution is not an issue. The electro-emission experiment is also useful when the absorption band occurs at energies below 400 nm—the approximate wavelength cutoff of the Stark cells used.

4. Experimental

4.1. 1-(2-Pyridyl)-3-(N,N′-diphenylaminobenzyl)propene-1-one

Twenty-five milliliter of 5% aqueous KOH was added to a solution of *N*,*N*′-diphenylaminobenzaldehyde (3.88 g, 14.2 mmol) in 50 ml methanol and 8 ml methylene chloride with vigorous stirring while cooling in an ice bath. 2-Acetylpyridine (2.6 g, 21.3 ml) in 20 ml anhydrous methanol was added dropwise to the mixture, again contained in an ice bath. The combined solution was stirred vigorously overnight. The resulting yellow–orange solution was poured into 200 ml of ice water and filtered to collect the yellow–orange precipitate, which was washed with water. The crude product was re-dissolved and extracted into methylene chloride. The organic layer was dried over $MgSO_4$ and filtered. After evaporation of solvent, the product was purified by flash chromatography on silica using 4:1 hexane + ethylacetate as eluent. After removal of solvent a red–orange solid was isolated in 64% yield (3.42 g). ^{1}H-NMR (CD_2Cl_2): $\delta = 8.73$ (s, 2H), 8.16 (d, 4H), 7.89 (d, 2H), 7.61 (d, 2H), 7.58 (d, 2H), 7.49 (d, 2H), 7.32 (m, 2H), 7.15 (m, 4H), 7.02 (m, 2H) ppm. ^{13}C-NMR (CD_2Cl_2): $\delta = 154.7$, 150.5, 149.1, 147.1, 144.3, 137.3, 130.3, 129.8, 128.4, 127.0, 126.7, 125.9, 125.5, 124.5, 122.9, 121.6, 118.5 ppm. Anal. Calc. for $C_{26}H_{20}N_2O$: C, 82.99; H, 5.32; N, 7.45. Found: C, 83.01; H, 5.29; N, 7.43%. MS (ESI): $m/z = 377$ [M^+].

4.2. DPA-tpy (1)

4′-(4-*N*,*N*′-Diphenylaminobenzyl)-2,2′:6′,2″-terpyridine (DPA-tpy) was prepared by a method similar to the method described by Mukkala et al., for substituted phenyl terpyridine compounds [20]. Briefly, 1-(2-pyridyl)-3-*N*,*N*′-diphenylaminobenzyl)propene-1-one (2.77 g, 7.36 mmol), 1-(2-pyridinylcarbonyl)pyridinium iodide (2.4 g, 7.36 mmol), and ammonium acetate (5.7 g, 78 mmol) were dissolved in anhydrous methanol (80 ml) and refluxed for 12 h under nitrogen. The dark brown mixture was allowed to cool to room temperature and the solvent was removed. The residue was dissolved in methylene chloride and neutralized with aqueous sodium bicarbonate. The organic layer was separated, dried over $MgSO_4$, and filtered. After removal of solvent, the isolated compound was chromatographed on activated neutral aluminum oxide (Aldrich) 4:6 ethylacetate + hexane as eluent. Yield: 1.6 g, 46%. ^{1}H-NMR (CD_2Cl_2): $\delta = 8.76$ (s, 2H), 8.71 (m, 4H), 7.90 (d, 2H), 7.81 (d, 2H), 7.33 (d, 2H), 7.19 (m, 4H), 7.11 (m, 4H) ppm. ^{13}C-NMR (CD_2Cl_2): $\delta = 156.4$, 156.2, 149.4, 147.6, 137.1, 136.7, 129.7, 128.3, 125.3, 125.2, 124.2, 123.8, 123.2, 121.4, 118.3 ppm. Anal. Calc. for $C_{33}H_{24}N_4$: C, 83.20; H, 5.04; N, 11.76. Found: C, 82.84; H, 4.76; N, 11.42%. MS (ESI): $m/z = 477$ [M^+].

4.3. [Co(DPA-tpy)$_2$](PF$_6$)$_2$ (2)

A mixture of $Co(NO_3)_2\cdot 6H_2O$ (20 mg, 0.068 mmol) and 1 (68 mg, 0.143 mmol) was refluxed for 3 h in a CH_3CN + ethanol mixture (1:1, 20 ml) then cooled to room temperature. Following solvent removal by rotary evaporation, the crude solid was dissolved in acetonitrile. Ethyl ether was then added to the solution with vigorous stirring, resulting in product precipitation. The product was filtered, successively washed with H_2O, ethanol, and diethylether, and air-dried. The crude dark brown product was subsequently purified by column chromatography over basic alumina (CH_2Cl_2 + CH_3CN), producing a red–brown eluent. The remaining residue following evaporation was dissolved in CH_3CN (10 ml), and precipitation of the product was achieved by adding a saturated aqueous KPF_6 solution. After filtering and successive washing with H_2O, cold ethanol, and diethylether, the product was further recrystallized

from CH_3CN+diethylether, giving a dark red–brown product (58 mg, 64% yield). Anal. Calc. for $C_{66}H_{48}N_8CoP_2F_{12}\cdot 1.2\ CH_3CN$: C, 60.81; H, 3.82; N, 9.54. Found: C, 60.80; H, 3.61; N, 9.21%. MS (ES): $m/z = 555.3$ $[M-2PF_6^-]^{2+}$.

4.4. [Co(DPA-tpy)$_2$](PF$_6$)$_3$ (3)

A mixture of $CoCl_2\cdot 6H_2O$ (75 mg, 0.315 mmol) and **1** (320 mg, 0.672 mmol) was refluxed for 3 h in a CH_3CN+ethanol mixture (1:1, 20 ml) then cooled to room temperature. Following solvent removal by rotary evaporation, the crude solid was recrystallized from a CH_3CN+diethylether mixture, producing a dark precipitate. This dark solid (180 mg) was dissolved in 0.1 M HCl (25 ml), to which PbO_2 (40 mg, 0.17 mmol) was added. The mixture was heated for 1 h and filtered. Precipitation of the product was achieved by adding a saturated aqueous $K(PF_6)$ solution to the vigorously stirred filtrate. The product was filtered, washed successively with H_2O and diethylether, and air-dried. Final recrystallization was from CH_3CN+diethylether, giving a red powder (140 mg, 30.7% yield). Anal. Calc. for $C_{66}H_{48}N_8CoP_3F_{18}\cdot 1.5H_2O$: C, 53.79; H, 3.46; N, 7.61. Found: C, 53.62; H, 3.01; N, 7.62%. MS (ES): $m/z =$ 1301.6 $[M-PF_6^-]^+$; 578 $[M-2PF_6^-]^{2+}$; 337 $[M-3PF_6^-]^{3+}$.

4.5. [Zn(DPA-tpy)$_2$](PF$_6$)$_2$ (4)

A mixture of $(CH_3CO_2)_2Zn\cdot 2H_2O$ (85 mg, 0.387 mmol) and **1** (380 mg, 0.798 mmol) was refluxed for 2 h in a dry tetrahydrofuran+$CHCl_3$ mixture (3:1, 40 ml) then cooled to room temperature. Following solvent removal by rotary evaporation, the residue was dissolved in acetonitrile (5 ml), and a saturated aqueous KPF_6 solution was added with vigorous stirring to precipitate the complex. The solid was filtered and washed successively with H_2O, cold ethanol, and diethylether. Product purification was identical to the procedure for **2**, and the final product was recrystallized from CH_3CN+diethylether (340 mg, 67% yield). Anal. Calc. for $C_{66}H_{48}N_8ZnP_2F_{12}\cdot CH_3CN$: C, 60.54; H, 3.78; N, 9.35. Found: C, 60.52; H, 3.61; N, 9.21%. MS (ES): $m/z = 1163$ $[M-PF_6^-]^+$; 508.6 $[M-2PF_6^-]^{2+}$.

4.6. Zn(DPA-tpy)Cl$_2$ (5)

A solution of **1** (0.48 g, 1.0 mmol) in CH_2Cl_2 (8 ml) was added to a solution of $ZnCl_2$ (0.136 g, 1.0 mmol) in dry ethanol (25 ml). The reaction mixture was refluxed for 3 h, then cooled to room temperature. The crude yellow precipitate was filtered and washed with ethanol and diethylether. The product was recrystallized from warm ethanol, giving a light yellow powder (380 mg, 62% yield). Anal. Calc. for $C_{33}H_{24}N_4ZnCl_2\cdot 0.5CH_3CH$: C, 64.23; H, 4.25; N, 8.81. Found: C, 64.20; H, 3.82; N, 8.85%. MS (ESI): $m/z = 612$ $[M^+]$.

4.7. Electric field-effect measurements

Stark absorption measurements were conducted on frozen butyronitrile solutions (77 K) using instrumentation previously described. Typical applied field strengths were ca. 3×10^7 V m^{-1}. Spectra were recorded at angles (χ) of 0° and 55°. At least four measurements were recorded at each angle, fit to Eq. (3), and used to determine average polarization and dipole moment changes.

Stark emission measurements were conducted at 77 K with polymethylmethacrylate (PMMA) thin films containing the compounds. Samples were prepared by dissolving the chromophore in a dichloroethane solution containing PMMA (Aldrich, $M_w \approx 996$ kD, 0.75 g/15 ml), passing the solution through a 0.22-μm teflon filter, drop casting a film in an aluminum dish and then drying the film overnight. Film thicknesses were determined by measuring the spacing of interference peaks in IR spectra of the films and were typically 180–200 μm [1]. Measurements were conducted using instrumentation and procedures previously described [4,5]. Typical applied field strengths were ca. 2×10^7 V m^{-1}, and all samples were excited at 350 nm. Again, spectra were recorded at angles (χ) of 0° and 55° between the incident electromagnetic field and the applied electrical field vectors. Two film samples were prepared and measured for each complex, with at least four measurements performed at each angle. The resulting calculated parameters were averaged to obtain the reported dipole moment and polarizability changes.

4.8. Other measurements

^{1}H- and ^{13}C-NMR spectra were recorded on a Varian Mercury 400 MHz spectrometer at 25 °C. Ambient temperature electronic absorption spectra were recorded in acetonitrile as solvent using an HP 8452A diode array spectrophotometer. Luminescence spectra of nitrogen-purged sample solutions were measured with an ISA Fluorolog Model FL3-11 spectrophotometer, with excitation at the sample's absorption maximum. Elemental analyses were performed by ORS, Oneida, NY.

4.9. Calculations

Semi-empirical electronic structure calculations were performed using Hyperchem 5.11. Geometry optimization was achieved using Polak-Ribere methodology and either AM1 (**1**, **4**, and **5**) or ZINDO/1 (**2** and **3**) parameters. Upon optimization, a final CI single-point calculation was performed on the ground state and lowest singlet excited state of the molecule to obtain

molecular orbital electronic distributions and both dipole moment and polarizability changes.

5. Results

5.1. Zero-field electronic spectra

Shown in Fig. 3 are ambient temperature electronic absorption and emission spectra for DPA-tpy (**1**) and four of its metal complexes: $Co^{II}(DPA\text{-}tpy)_2^{2+}$ (**2**), $Co^{III}(DPA\text{-}tpy)_2^{3+}$ (**3**), $Zn^{II}(DPA\text{-}tpy)_2^{2+}$ (**4**), and $Zn^{II}(DPA\text{-}tpy)(Cl)_2$ (**5**). The absorption spectrum of **1** features a reasonably intense near-UV band that is absent from spectra for the component electron donor and acceptor species. The band is assigned to the intramolecular charge transfer process shown in Eq. (1). As observed for related bipyridine- and terpyridine-based donor–acceptor compounds, metal cation coordination tends to shift the charge transfer band to lower energy [21–23]. The exception is the neutral compound, **5**. The red shift observed for **2**, **3**, and **4** is primarily an electrostatic effect; the positive charge of the coordinated cation serves to stabilize the photo-generated terpyridine anion fragment. Especially for Zn(II), which is a closed-shell d^{10} ion, interactions with metal d orbitals can be neglected. Consistent with the electrostatic explanation the charge transfer band for the tripositive cobalt complex is significantly red shifted with respect to the di-positive complex, **2**.

The breadth of the emission spectra for compounds **1**, **2**, **4** and **5** (compound **3** is non-emissive) and the energetic proximity of the bands to the corresponding charge transfer absorption bands suggests assignment of the emissions as charge transfer transitions—a conclusion that is corroborated by Stark measurements. In contrast, terpyridine-localized emission spectra are structured and occur at higher energy than found here.

5.2. Stark absorption spectra

Panels c and d of Fig. 4 show typical electroabsorption spectra—in this case for compound **5** at $\chi = 0°$ and 55°, respectively. For comparison, panels a and b show the low-temperature absorption spectrum (zero-field

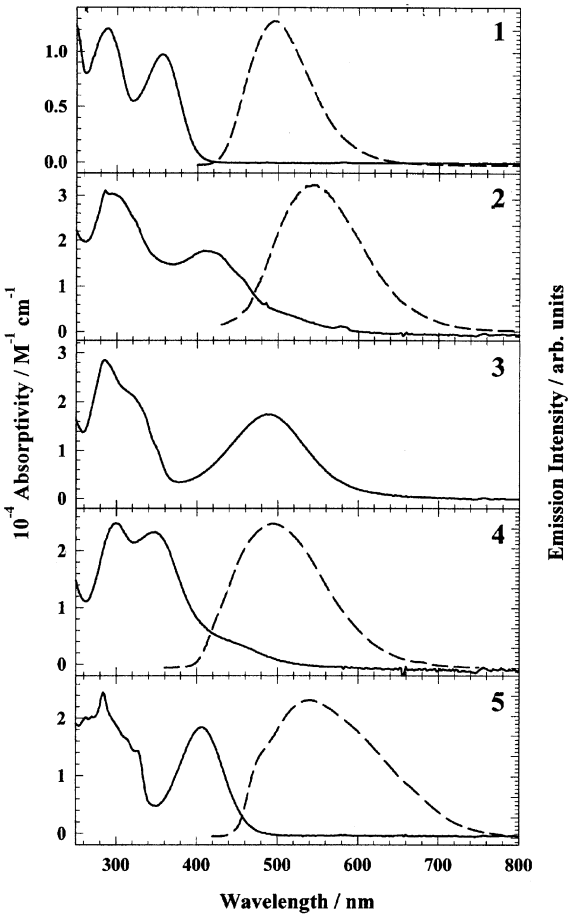

Fig. 3. Electronic absorption (solid line) and emission (dashed line) spectra for compounds **1**–**5** at 298 K in deoxygenated acetonitrile as solvent.

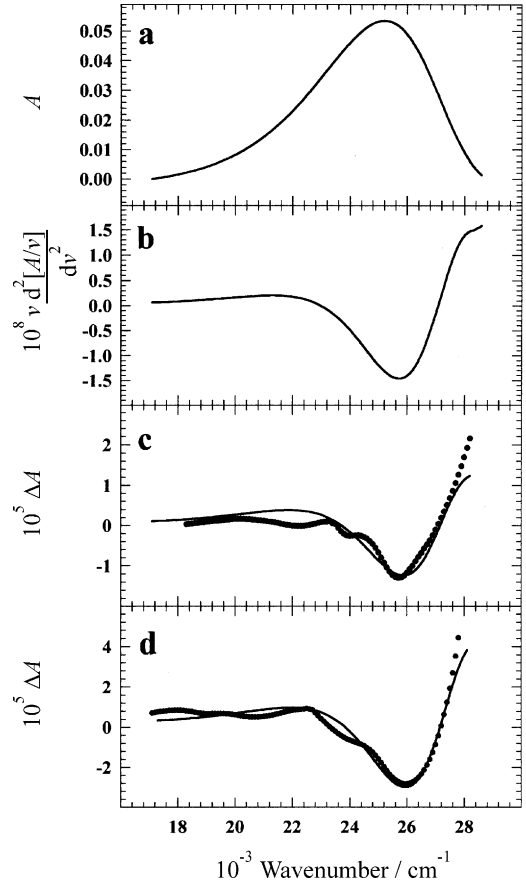

Fig. 4. *Panel a:* Absorption spectrum of compound **5** in a butyronitrile glass at 77 K. *Panel b:* Energy normalized (see Eq. (3)) numerical second-derivative of the absorption spectrum. *Panel c:* Experimental electroabsorption spectrum (dots) and best-fit spectrum using Eq. (3) (dashes). $\chi = 0°$. *Panel d:* Same as panel c, except at $\chi = 55°$.

spectrum) and its second-derivative. The qualitative similarity of the Stark lineshape to the second-derivative of the zero-field spectrum indicates that the change in dipole moment upon optical excitation is the primary contributor to the Stark spectrum. Fits to Eq. (2) (solid lines in panels c and d) yield a $|\Delta\mu|$ value of 18 Debye. As shown by Cave and Newton [18], the change in dipole moment is identical to the product of the unit electronic charge and the adiabatic charge transfer distance, R_{12}:

$$|\Delta\mu| = eR_{12} \quad (7)$$

For compound **5** the internal ET distance is 3.7 Å where 1 eÅ = 4.8 Debye. For comparison, the distance from the amine nitrogen (donor site) to the closest terpyridyl nitrogen (acceptor site) is 8.4 Å. The trace of the polarizability change for 5 is 100 Å^3. Table 1 lists $|\Delta\mu|$ and Tr$\Delta\alpha$ data for charge transfer within compounds **2** and **3**. For all three compounds the fits give ξ values close to zero. Data were unattainable for **1** and **4** because these absorb too far to the blue.

5.3. Stark emission spectra

Fig. 5 shows Stark emission spectra for compound **5**. Again note the similarity of the spectra to the second-derivative of the zero-field spectrum. As in the electro-absorption experiment this signals the importance of dipole moment changes. Fits to the Stark spectra yield $|\Delta\mu| = 4.7$ eÅ and Tr$\Delta\alpha = 960$ Å^3. Table 1 summarizes the Stark emission data for all compounds but **3**. For compound **5** the charge transfer distance measured by absorption versus emission differs by slightly more than the estimated measurement uncertainties (ca. 10% for each). The differences might reflect, in part, small differences in the local field correction factors, f. While we have assumed they are identical for butyronitrile glass and PMMA matrices, work by Bublitz and Boxer indicates that f values can differ slightly if matrices have differing polarities [24]. Another possibility is that the distances indeed do vary in the two experiments. The absorption measurement samples the Franck-Condon region of the upper electronic surface, while the emission experiment involves a vibrationally relaxed upper electronic state (charge transfer state)—the difference, of course, accounting for half the observed absorption/emission Stokes shift. If the extent of charge transfer depends in some fashion on the magnitude of the ground state/excited state energy gap—or perhaps more likely, on the gap between the charge transfer state and higher electronic states lacking charge transfer

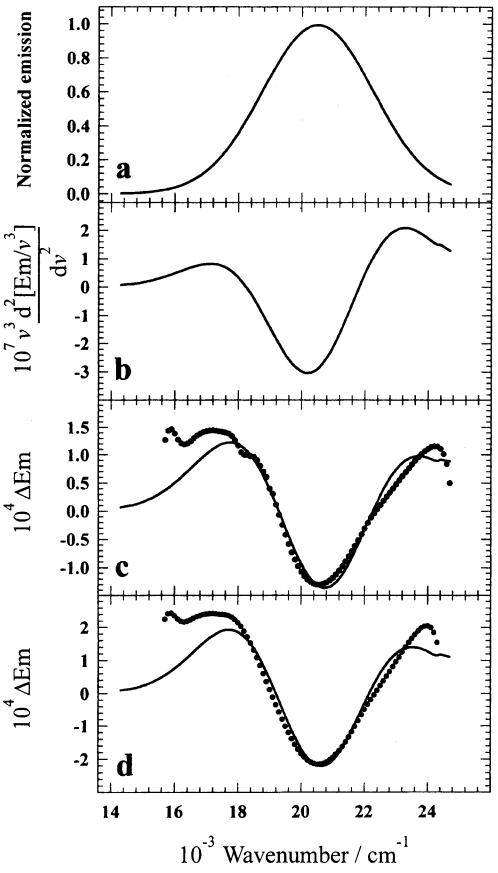

Fig. 5. *Panel a:* Emission spectrum for compound **5** in a PMMA thin film at 77 K. *Panel b:* Energy normalized numerical second-derivative of emission spectrum. *Panel c:* Experimental electro-emission spectrum (dots) and best-fit spectrum (dashes) at $\chi = 0°$. *Panel d:* Same as panel c, except at $\chi = 55°$.

Table 1
Stark spectroscopy and ET distance parameters

Compound	$\|\Delta\mu$(abs)$\|$/Debye	Tr$\Delta\alpha$(abs)/Å^3	$\|\Delta\mu$(em)$\|$/Debye	Tr$\Delta\alpha$(em)/Å3	R_{12}/Å [a]	R_{ab}/Å [b]	$\Delta q/e$ [c]
DPA-tpy (**1**)	–	–	9	200	1.9	2.4	0.8
Co(DPA-tpy)22+ (**2**)	13	150	14	600	2.9	3.8	0.7
Co(DPA-tpy)23+ (**3**)	21	150	–	–	4.3	5.0	0.7
Zn(DPA-tpy)22+ (**4**)	–	–	17	800	3.5	4.3	0.8
Zn(DPA-tpy)Cl2 (**5**)	18	100	23	950	4.2	4.7	0.9

[a] Adiabatic charge transfer distance taken from the average of Stark absorption and emission measurements of the absolute change in dipole moment.
[b] Nonadiabatic charge transfer distance calculated from R_{12} and the integrated charge transfer absorption band; Eqs. (8)–(10).
[c] Fractional amount of charge transferred from donor site to acceptor site upon optical excitation.

character—this would be manifest as a difference in the adiabatic charge transfer distance in the absorption versus emission process.

The emission analysis also returns different values for the change in polarizability. It is unclear whether the differences represent real physical differences in the absorption versus emission process, or instead reflect a bias in one or both measurements. In any case, the first-derivative component (change-in-polarizability component) is a minor component of both fits; we will focus for the remainder of the paper on the second-derivative component (change-in-dipole-moment component). *A*-term contributions comprised negligible components of the fit spectra.

6. Discussion

From Table 1 the measured adiabatic ET distances are: (a) significantly shorter than the geometric donor/acceptor separation distance, R_{geo} ($=8.4$ Å via molecular modeling), and (b) significantly altered (lengthened) by cation coordination, with the lengthening effect being greater for a more highly charged cation. One factor potentially accounting for an apparently shorter than geometric distance for ET is transfer of less than a full electronic charge (e)—a not unreasonable assumption for a covalently linked donor/acceptor pair. Cave and Newton have pointed out that the following relationship holds:

$$eR_{12} = \Delta q R_{ab} \tag{8}$$

where Δq is the actual amount of charge transferred and R_{ab} is the nonadiabatic ET distance [18]. In the two-state limit, R_{ab} can be estimated from:

$$eR_{ab} = [(\Delta\mu)^2 + 4\mu_{12}^2]^{1/2} \tag{9}$$

where μ_{12} is the transition dipole moment. As indicated in Eq. (10), the transition dipole moment scales as the integrated intensity of the charge transfer absorption band:

$$\mu_{12} = 2.03 \times 10^{-2}(\varepsilon_{max}\Delta\nu_{1/2}/\nu_{max})^{1/2} \tag{10}$$

In Eq. (10), which assumes a gaussian lineshape, ε_{max} is the maximum extinction coefficient of the charge transfer absorption, $\Delta\nu_{1/2}$ is the band width at half height, and ν_{max} is the energy at the absorption maximum.

We have applied Eqs. (8)–(10) to the five available donor/acceptor systems and have summarized the results in Table 1. For **2**, **3** and **4** we took into account the presence of two chromophores per complex. It is clear from the analysis that partial charge transfer can account for only a minor component (0.2–0.5 Å) of the difference between R_{12} and R_{geo}.

Another possibility is self-polarization in the charge-separated state. Briefly, a positively charged hole created on the original donor can exert a coulombic pull on the transferred electron and vice versa, resulting in a shortening of the ET. Furthermore, the hole can also interact coulombically with other valence electrons, slightly displacing them from their original positions and likewise pulling them toward itself. Since our analysis is based upon a one-electron description, any displacement of other valence electrons will evince an apparent additional displacement of the transferred electron. (For example, a displacement of each of 20 electrons by 0.1 Å is electrostatically equivalent to displacement of the transferred electron by 2 Å and will be read out as such in a one-electron analysis of experimental measurements.)

To gain insight into self-polarization and related effects, we carried out electronic structure calculations (semi-empirical calculations) on the ground- and charge-transfer excited state of the donor/acceptor compound and one of its complexes (**5**). The calculated distances are in relatively poor quantitative agreement with experiment: R_{12}(calc) = 1.1 and 1.8 Å for light-induced ET within **1** and **5**, respectively. One factor may be the neglect of solvent, which would otherwise stabilize the charge transfer state and probably increase the calculated transfer distances. The calculations, however, do agree qualitatively with the experimental observations that real ET distances are shorter than geometric separation distances and that cation coordination by the electron-acceptor lengthens the transfer distance. Further qualitative insight can be gained by examining the calculated HOMO and LUMO shapes, as defined by fixed electron density contours of the frontier orbital electron density in the ground and excited state, respectively. Fig. 6 shows the orbital shapes for compound **1**. As one would expect, the HOMO is largely centered around the amine nitrogen and constituent

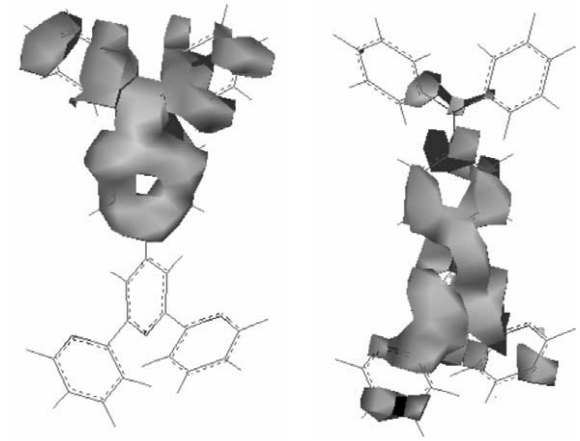

(a) (b)

Fig. 6. Electron density for the (a) HOMO and (b) LUMO of **1**, determined via semi-empirical calculations.

phenyl groups. The LUMO, on the other hand, encompasses not only the terpyridine nitrogen atoms and associated aromatic rings, but also portions of the phenyl group linking the nominal acceptor unit (terpyridine) to the amine donor. Extension of electron density onto the phenyl link no doubt accounts for a significant portion of the reduction in real ET distance relative to the geometric donor/acceptor separation distance.

Fig. 7 presents similar data for system **5**. From the figure, the HOMO shape is only slightly changed by metal cation coordination. For the LUMO, however, cation binding substantially alters the shape, largely eliminating orbital delocalization onto the phenyl linking group and redistributing portions of the orbital onto the more distant terpyridine unit. While the calculated HOMO and LUMO shapes cannot be equated directly with ground- and excited-state charge distributions, they do strongly imply that lengthening of the ET distance upon metal ion coordination is primarily associated with a coulombic redistribution of charge in the ET product state rather than reactant state. Although we have not performed such calculations, an amplification of the product-state redistribution effect upon replacement of a di-cation by a tri-cation probably accounts for the greater ET distance found for **3** versus **2**.

7. Conclusions

Appplication of electric field-effect spectroscopies to light-induced ET within a covalently linked donor/acceptor assembly and several of its coordination complexes yields experimental ET distances that are much smaller than the geometric donor site/acceptor site separation distance. Especially for the metal-free assembly, the reduced transfer distance appears to be associated with delocalization of charge in the product state back onto the original donor. Another factor is the tendency to transfer less than a full electronic charge in strongly interacting systems such as **1**, since the quantity returned by the experiment is the product of the unit electronic charge and the adiabatic transfer distance. If instead the nonadiabatic transfer distance is recovered from the experiment (in other words, if the apparent effect of transferring only a fraction of a charge is taken into account), the measured distances increase by ca. 10–25%. These values still fall short, however, of the geometric separation distance. Complexation of di-positive or tri-positive metal cations by the electron-acceptor portion of the assembly causes the intramolecular ET distance to increase substantially, even though the chemical identity of the acceptor has not been altered. The effect is greater for coordination of a triply charged cation than for one that is doubly charged and is observed both with open-shell and closed-shell ions. The lengthening of the transfer distance is an electrostatic effect that appears to be associated primarily with a reduction in the size of the orbital occupied by the transferred electron in the product state.

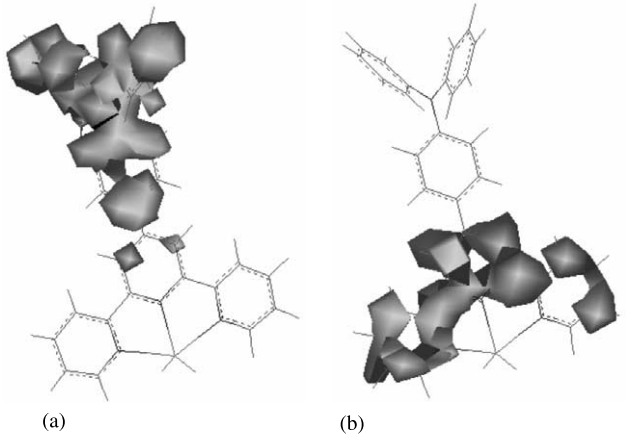

Fig. 7. Electron density for the (a) HOMO and (b) LUMO of **5**, determined via semi-empirical calculations.

Acknowledgements

JTH gratefully acknowledges Mike Weaver's mentorship and formative influence upon his career as a scientist. We thank the Office of Science, U.S. Dept. of Energy under grant no. 87ER-13808 for support of our work.

References

[1] M.J. Weaver, H.Y. Liu, Y. Kim, Can. J. Chem. 59 (1984) 1953.
[2] T.T. Li, M.J. Weaver, J. Am. Chem. Soc. 106 (1984) 6107.
[3] M.J. Weaver, G.E. Mcmanis, Acc. Chem. Res. 23 (1990) 294.
[4] D.H. Oh, M. Sano, S.G. Boxer, J. Am. Chem. Soc. 113 (1991) 6880.
[5] B.J. Coe, J.A. Harris, B.S. Brunschwig, J. Phys. Chem. A 106 (2002) 897.
[6] G.U. Bublitz, R. Ortiz, S.R. Marder, S.G. Boxer, J. Am. Chem. Soc. 119 (1997) 3365.
[7] F.W. Vance, R.D. Williams, J.T. Hupp, Int. Rev. Phys. Chem. 17 (1998) 307.
[8] K.A. Walters, Y. Kim, J.T. Hupp, Inorg. Chem. 41 (2002) 2909.
[9] L. Karki, J.T. Hupp, Inorg. Chem. 36 (1997) 3318.
[10] F.W. Vance, R.V. Slone, C.L. Stern, J.T. Hupp, Chem. Phys. 253 (2000) 313.
[11] R.C. Johnson, J.T. Hupp, J. Am. Chem. Soc. 123 (2001) 2053.
[12] S.F. Nelsen, M.D. Newton, J. Phys. Chem. A 104 (2000) 10023.
[13] Y.K. Shin, B.S. Brunschwig, C. Creutz, N. Sutin, J. Phys. Chem. 100 (1996) 8157.
[14] B.S. Brunschwig, C. Creutz, N. Sutin, Coord. Chem. Rev. 177 (1998) 61.
[15] J.R. Reimers, N.S. Hush, J. Phys. Chem. 95 (1991) 9773.
[16] K. Senechal, O. Maury, H. Le Bozec, I. Ledoux, J. Zyss, J. Am. Chem. Soc. 124 (2002) 4560.

[17] W. Liptay, in: E.C. Lim (Ed.), Excited States, Academic Press, New York, 1974.
[18] R.J. Cave, M.D. Newton, Chem. Phys. Lett. 249 (1996) 15.
[19] M. Ponder, R.A. Matthies, J. Phys. Chem. 87 (1983) 5090.
[20] V.A. Mukkala, M. Helenius, I. Hemmila, J. Kankare, H. Takalo, Helv. Chim. Acta 76 (1993) 1361.
[21] F.W. Vance, J.T. Hupp, J. Am. Chem. Soc. 121 (1999) 4047.
[22] J.F. Michalec, S.A. Bejune, D.G. Cuttell, G.C. Summerton, J.A. Gertenbach, J.S. Field, R.J. Haines, D.R. McMillin, Inorg. Chem. 40 (2001) 2193.
[23] N.W. Armaroli, L. De Cola, V. Balzani, J.P. Sauvage, C.O. Dietrich-Buchecker, J.M. Kern, J. Chem. Soc., Faraday Trans. 88 (1992) 553.
[24] G.U. Bublitz, S.G. Boxer, J. Am. Chem. Soc. 120 (1998) 3988.